IEEE Access
Multidisciplinary | Rapid Review | Open Access Journal

Received March 8, 2019, accepted March 13, 2019, date of publication March 18, 2019, date of current version April 11, 2019.

Digital Object Identifier 10.1109/ACCESS.2019.2905648

A Narrowband Anti-Jamming Acquisition Algorithm Based on All-Phase Processing for BOC Signals

YI PAN, TIANQI ZHANG, GANG ZHANG, AND ZHONGTAO LUO

School of Telecommunication and Information Engineering, Chongqing University of Posts and Telecommunications, Chongqing 400065, China

Corresponding author: Yi Pan (willboc@126.com)

This work was supported in part by the Natural Science Foundation of China under Grant 61671095, Grant 61702065, Grant 61701067, and Grant 61771085, in part by the Project of Key Laboratory of Signal and Information Processing of Chongqing under Grant CSTC2009CA2003, in part by the Chongqing Graduate Research and Innovation Project under Grant CYS17219, and in part by the Research Project of the Chongqing Educational Commission under Grant KJ1600427 and Grant KJ1600429.

ABSTRACT The accuracy transmission of a binary offset carrier (BOC) signal is always affected by narrowband interference (NBI), and a novel anti-jamming acquisition algorithm based on all-phase processing finite impulse response (apFIR) and partially matched filter-all phase fast Fourier transform (PMF-apFFT) is proposed in this paper. First, an apFIR filter with precise settings for arbitrary notch points was constructed, and then the PMF-apFFT method was adopted to achieve the acquisition of the contaminated BOC signals. Simulation and analysis show that the proposed algorithm can effectively suppress NBI and simultaneously complete correct pseudo-random (PN) phase search and accurate Doppler frequency estimation, and it shows superior performance in mean square error (MSE) and detection probability.

INDEX TERMS Binary offset carrier (BOC) signal, acquisition, narrowband interference (NBI), all-phase processing.

I. INTRODUCTION

Binary offset carrier (BOC) signals have been widely used in global satellite navigation systems (GNSS), but the subcarrier modulation of BOC signals results in the multi-peak characteristics of autocorrelation function and the split spectrum characteristics of power spectrum. Several acquisition algorithms were proposed to solve ambiguous problem [1]–[4]. Also, in real-world communication system, besides the background noise, BOC signals are susceptible to the interference from natural or artificial signals, whose frequency might be located in the satellite signal bands. In the case of strong narrowband interference, limited by bandwidth and system frequency resources, the spread spectrum gain cannot be very high, causing the performance of receiver deteriorates sharply or even fail to run normally [5], [6]. The narrowband anti-jamming technique for acquisition has been proposed in the context of Global Positioning System (GPS) C/A signal in both theory and experiments [7]. However, narrowband anti-jamming techniques for BOC signal, which shares the same frequency band with GPS C/A signal, have not been studied much yet.

Narrowband anti-jamming techniques can usually be divided into three categories, space filtering, time-domain filtering, transform-domain filtering. Spatial filtering [8], [9] can mitigate both wideband and narrowband jamming. However, it requires additional hardware to the GPS receiver. Time-domain filtering [10], [11] suppresses narrowband interference (NBI) according to the different predictable characteristics of spread spectrum signals and jamming signals. When the communication environment is relatively stable, its ability of anti-jamming is strong. But when jamming signal changes quick, time-domain algorithm has the problem of convergence speed. Additionally, it is difficult to complete the calculation in a relatively fast time for the receiver as the signal rate is relatively fast, which is not suitable for real-time systems. And if there are strong correlations among spread spectrum signals, this method is not applicable. Transform-domain filtering [12]–[17] takes advantages of spread spectrum signals and jamming signals having different mapping characteristics in the same transform domain, and realizes complex filtering in time domain by simple multiplication.

The associate editor coordinating the review of this manuscript and approving it for publication was Fang Yang.

$$\mathbf{D}=\begin{bmatrix} x(n) & x(n+1) & x(n+2) & \dots & x(n+N-1) \\ x(n-1) & x(n) & x(n+1) & \dots & x(n+N-2) \\ x(n-2) & x(n-1) & x(n) & \dots & x(n+N-3) \\ & & \vdots & & \\ x(n-N+1) & x(n-N+2) & x(n-N+3) & \dots & x(n) \end{bmatrix} \tag{8}$$

It can even realize some filtering which cannot be realized in time domain, such as ideal bandpass and bandstop filters. To ensure that the original signal can be restored, the transformation must be reversible. Furthermore, due to that no convergence for interference suppression in the frequency-domain filtering, the processing speed in the receiver is very fast, which can meet the real-time requirements of acquisition.

According to the different ways of signal transformation, frequency-domain filtering can be divided into Short Time Fourier Transform (STFT) [12], Wavelet Packet Transform (WPT) [13], Compressed Sensing (CS) [14], [15] and Fast Fourier Transform (FFT) [16], [17]. Among them, the anti-jamming technique based on FFT has been widely used in engineering for its simple implementation, small hardware cost and fast speed. However, spectrum leakage often exists in FFT operation, and overlapping window (OW) [17] is often used to solve this problem. In order to further suppress the spectrum leakage, all-phase processing [18], [19] is adopted.

In this paper, the sampled BOC signal was traversed all possible positions and multiplied with all-phase processing Finite Impulse Response (apFIR) filter coefficient h(n), and then an adaptive threshold method was adopted to determine the parameters for notch. For the acquisition stage, the partial matched filter (PMF)-all phase Fast Fourier Transform (apFFT) algorithm was used to realize the acquisition of BOC signals. The organization of this paper is as follows. Section II formalizes the BOC modulated signal model, the exact expressions of the design of apFIR filter, the adaptive threshold and the output of PMF-apFFT. Section III presents the specific process of narrowband anti-jamming and the acquisition scheme, an efficient structure diagram for the proposed method is presented as well. In Section IV, the feasibility and availability of the proposed method with the comparison between the performance of its and others are shown and discussed. Finally, conclusions as well as the applicable scene are discussed in Section V.

II. SIGNAL MODEL AND ACQUISITION PRINCIPLE

A. PRELIMINARIES

After filtering and amplification, a radio frequency (RF) signal is down-converted to an intermediate frequency (IF) signal by a mixer, and the received BOC signal can be expressed as

$$r(t)=Ad(t)s(t)\cos\left(\left(f_{IF}+f_d\right)t+\phi_0\right)+n(t) \tag{1}$$

where A is the amplitude of signal; $d(t)$ is navigation data; f_{IF} is intermediate frequency; f_d is Doppler frequency; ϕ_0 is the initial phase of the carrier; $n(t)$ is White Gaussian noise with zero-mean and variance σ_{n}^2. $s(t)$ is BOC baseband signal, which can be expressed as

$$s(t)=c(t)\,sc(t) \tag{2}$$

where $sc(t)=\mathrm{sgn}[\sin(2\pi f_{sc}t)]$ is the subcarrier with the frequency f_{sc} and the period T_{sc}, sgn(x) is the sign function, which takes the value of 1 for x >0 and -1 for x <0. $c(t)$ is the spreading code, and can be defined as

$$c(t)=\sum_{i=-\infty}^{\infty}c_i p_{T_c}(t-iT_c) \tag{3}$$

where $c_i\in\{-1,1\}$ is the ith chip of a pseudo-random (PN) code. $p_\alpha(t)$ is the PN code waveform, which is a rectangular pulse over $[0,\alpha)$, T_c is the chip period of PN code.

The contaminated BOC signal is given by

$$x(t)=r(t)+J(t)+n(t) \tag{4}$$

where $J(t)$ is multi-tone jamming, which can be defined as

$$J(t)=\sum_{k=1}^{K}A_k\sin(\omega_k t+\theta_k) \tag{5}$$

where K is the number of single-tone jamming, A_k is the amplitude of kth interference signal, ω_k is the angular frequency of kth interference signal, θ_k is the random phase uniform distributed in $[0,2\pi]$. After sampling, the discrete form of contaminated BOC signal is obtained by

$$\mathbf{x}=\mathbf{r}+\mathbf{J}+\mathbf{n} \tag{6}$$

B. DESIGN OF ALL-PHASE FIR FILTER

The reason of spectrum leakage is that the data truncation is implied in FFT operation, which destroys the continuity of data. The traditional window function can reduce the side-lobe leakage range to a certain extent, but the suppression range is not large enough. All-phase processing, on the other hand, has a superior performance in mitigating the spectrum leakage, and the waveform distortion can be improved as well.

In order to get the N points all phase preprocessing data, the contaminated BOC signal is sampled for $2N-1$ points and can be rewritten as a row vector

$$\mathbf{x}=[x(n+N-1),\dots,x(n),\dots,x(n-N+1)] \tag{7}$$

The sampled data $\mathbf{x}$ of length $2N-1$ is divided into N segments, and each has a length of N. A N^*N data matrix $\mathbf{D}$ is given by all the truncation of central sampling data $x(n)$ in (8), as shown at the top of this page.

The elements of each row are cyclic shifted until center data $x(n)$ is moved to the first place in each row, the matrix $\mathbf{D}$ can be rewritten as

$$\mathbf{D} = \begin{bmatrix} x(n) & x(n+1) & \dots & x(n+N-2) & x(n+N-1) \\ x(n) & x(n+1) & \dots & x(n+N-2) & x(n-1) \\ & & \vdots & & \\ x(n) & x(n+1) & \dots & x(n-2) & x(n-1) \\ x(n) & x(n-N+1) & \dots & x(n-2) & x(n-1) \end{bmatrix} \tag{9}$$

The elements of matrix $\mathbf{D}$ in Equation (9) are added by corresponding column, the results are defined as follows

$$\begin{aligned} \mathbf{x}_{ap}(1) &= x(n) \\ \mathbf{x}_{ap}(2) &= (N-1)x(n+1) + x(n-N+1) \\ &\vdots \\ \mathbf{x}_{ap}(N) &= (N-1)x(n-1) + x(n+N-1) \end{aligned} \tag{10}$$

After all phase processing and normalizing, row vector $\mathbf{x}_{ap}$ can be expressed as

$$\mathbf{x}_{ap} = \frac{1}{N}[Nx(n), (N-1)x(n+1) + x(n-N+1), \cdots, x(n+N-1) + (N-1)x(n-1)] \tag{11}$$

The sequence $\mathbf{x}$ with length of $2N-1$ is transformed into the sequence $\mathbf{x}_{ap}$ with length of N by all-phase processing. The sequence $\mathbf{x}_{ap}$ can be regarded as the result of sequence $\mathbf{x}$ weighted by convolution window $w(n)$ and then added by the part of the overlapped data. The convolution window $w(n)$ is the convolution form of the front window $f(n)$ and the inverted rear window $e(n)$, and can be expressed as

$$\begin{aligned} w(n) &= f(n) * e(n) \\ &= \begin{cases} \sum_{k=0}^{N-1-n} e_k f_{k+n}, & n \in [0, N-1] \\ \sum_{k=-n}^{N-1} e_k f_{k+n}, & n \in [0, N-1] \\ 0, & n \in others \end{cases} \end{aligned} \tag{12}$$

where $f(n)$ and $b(n)$ are general window functions of length N. In order to keep the amplitude of input sequence and output sequence from deviating, the convolution window $w(n)$ should be normalized in practice. The central element $w(0)$ of the convolution window can be chosen as the normalization factor C

$$C = w(0) = \sum_{m=0}^{N-1} b_m f_m \tag{13}$$

The NBI signals mixed in the BOC signal are usually random and need to be suppressed as much as possible. Therefore, the design method of FIR notch filter can be generally adopted, which should be able to realize the gap of the frequency in the transmission function. In addition, the attenuation at the notch frequency should be large enough, also the design should be simple and the calculation should be small. In this paper, all-phase processing FIR (apFIR) filter based on dual phase shift is adopted. Firstly, two sub-filters are designed by all-phase processing, then they are phase-shifted in the opposite direction and adjusted by direct-current (DC) component, and NBI signal can be suppressed at any frequency by adjusting the parameters obtained from adaptive threshold algorithm. Assuming that the frequency vector is $\mathbf{H}$ and the value is set to zero at the position where the notch is needed, the design is normally carried out with a single window. $\mathbf{H}$ is a vector with even symmetry property

$$H(k) = H(M-1-k) \qquad k = 0, 1, \dots, M-1 \tag{14}$$

where M is the length of $\mathbf{H}$. The relationship between $H(k)$ and $w_k = 2k\pi/M$ is one-to-one correspondence, $\mathbf{H}$ is set to zero at $(l+1)$ and $(M-l+1)$

$$H(k) = \begin{cases} 0 & k = l, M-l \\ 1 & others \end{cases} \qquad 0 \le k \le M-1 \tag{15}$$

where l is a natural number.

Generally, the filter is implemented by increasing the order M for any point spectrum notching, apFIR filter based on dual phase shift is implemented by constructing two sub-notch vectors $\mathbf{H}_1$ and $\mathbf{H}_2$

$$H_1(k) = \begin{cases} 0 & k = l \\ 1 & others \end{cases} \qquad 0 \le l \le \left\lfloor \frac{M}{2} \right\rfloor - 1 \tag{16}$$

$$H_2(k) = \begin{cases} 0 & k = M-l \\ 1 & others \end{cases} \qquad 0 \le l \le \left\lfloor \frac{M}{2} \right\rfloor - 1 \tag{17}$$

where $\lfloor a \rfloor$ represents the biggest integer that is not bigger than a. There is only one notch point in $\mathbf{H}_1$, locating in the first half of the vector. The notch point in $\mathbf{H}_2$ is also in the second half of the vector, so the notch points of $\mathbf{H}_1$ and $\mathbf{H}_2$ are limited to $(0, \pi)$ and $(\pi, 2\pi)$, respectively

$$H_1(k) = H_2(M-k) \qquad k = 1, \dots, M-1 \tag{18}$$

It can be introduced the conjugation relations between $\mathbf{H}_1$ and $\mathbf{H}_2$ in time-domain

$$h_1^*(n) = h_2(n) \qquad n = 0, 1, \dots, M-1 \tag{19}$$

The IDFT for $\mathbf{H}_1$, $h_1(n)$ can be defined as

$$\begin{aligned} h_1(n) &= \frac{1}{M} \sum_{k=0}^{M-1} H_1(k) e^{j2\pi kn/M} \\ &= \frac{1}{M} \left[\left(\sum_{k=0}^{M-1} e^{j2\pi kn/M} \right) - e^{j2\pi ln/M} \right] \\ &= \begin{cases} -\dfrac{e^{j2\pi ln/M}}{M} & n \in [-M+1, -1] \cup [1, M-1] \\ \dfrac{(M-1)}{M} & n = 0 \end{cases} \end{aligned} \tag{20}$$

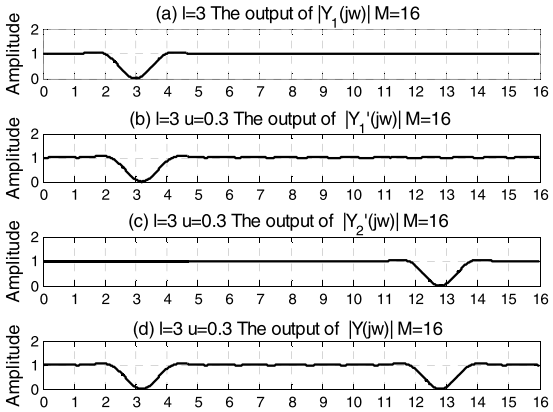

FIGURE 1. The curves of system function. (a) $|Y_1(j\omega)|$; (b) $|Y_1'(j\omega)|$; (c) $|Y_2'(j\omega)|$; (d) $|Y(j\omega)|$.

Using Hamming window $w(n)$, the output of subfilter is expressed as

$$\begin{aligned} y_1(n) &= \frac{1}{C} w(n) \cdot h_1(n) \\ &= \frac{1}{MC} w(n) \sum_{k=0}^{M-1} H_1(k) e^{j2\pi kn/M} \\ &= \begin{cases} -\dfrac{w(n) \cdot e^{j2\pi ln/M}}{MC} & n \in [-M+1,-1] \cup [1, M-1] \\ \dfrac{(M-1)}{M} & n = 0 \end{cases} \end{aligned} \tag{21}$$

In order to achieve the notch at any point, a phase shift $u_1(n)$ is constructed by

$$u_1(n) = e^{j2\pi \mu n/M} \quad n = [-M+1, M-1] \tag{22}$$

where μ is a constant, the output of phase shifted subfilter $y_1'(n)$ can be expressed as

$$\begin{aligned} y_1'(n) &= y_1(n) u_1(n) = y_1(n) \cdot e^{j2\pi \mu n/M} \\ &= \begin{cases} -\dfrac{w(n) \cdot e^{j2\pi(\mu - l)n/M}}{MC} \\ \quad n \in [-M+1,-1] \cup [1, M-1] \\ \dfrac{(M-1)}{M} \quad n = 0 \end{cases} \end{aligned} \tag{23}$$

The relationship between the system function $Y_1'(j\omega)$ and the original system function $Y_1(j\omega)$ is obtained as follows

$$Y_1'(j\omega) = Y_1\left[j\left(\omega + \frac{2\pi\mu}{M}\right)\right] \tag{24}$$

According to selection of parameter l, the location of the notch within $(0, \pi)$ is roughly determined. By adjusting the parameter μ, the notch at any frequency in $Y_1'(j\omega)$ can be realized, which effectively improves the accuracy of notch and prevents the energy loss caused by the large notch range. Figure1a and Figure 1b are the curves of $|Y_1(j\omega)|$ and $|Y_1'(j\omega)|$ respectively, where $l = 3$ and $\mu = 0.3$.

Derived from Equation (19) that

$$y_2(n) = [y_1(n)]^* \quad n = [-M+1, M-1] \tag{25}$$

And the phase shift vector $u_2(n)$ is conjugate to $u_1(n)$, similarly, the output of phase shifted subfilter $y_2'(n)$ can be expressed as

$$\begin{aligned} y_2'(n) &= y_2(n) u_2(n) = y_2(n) \cdot e^{-j2\pi \mu n/M} \\ &= \begin{cases} -\dfrac{w(n) \cdot e^{j2\pi(\mu+l-M)n/M}}{M} \\ \quad n \in [-M+1,-1] \cup [1, M-1] \\ \dfrac{(M-1)}{M} \quad n = 0 \end{cases} \end{aligned} \tag{26}$$

Adding $y_1'(n)$ to $y_2'(n)$ and subtracting a DC term with the magnitude of 1, the output of filter can be expressed as

$$\begin{aligned} y(n) &= \begin{cases} y_1'(n) + y_2'(n) \\ \quad n \in [-M+1, -1] \cup [1, M-1] \\ y_1'(0) + y_2'(0) - 1 \quad n = 0 \end{cases} \\ &= \begin{cases} -\dfrac{2w(n)}{MC} \cos\left[\dfrac{2(l-\mu)n\pi}{M}\right] \\ \quad n \in [-M+1, -1] \cup [1, M-1] \\ \dfrac{(M-2)}{M} \quad n = 0 \end{cases} \end{aligned} \tag{27}$$

Figure 1c and Figure 1d are the output curves of $|Y_2'(j\omega)|$ and $|Y(j\omega)|$ respectively, where $l = 3$ and $\mu = 0.3$.

Figure 2 shows the structure of a single-window apFIR filter, it can be seen that, an apFIR filter consists of N conventional FIR filters with N-order, thus is equivalent to a $2N-1$-order linear phase FIR filter. There are $2N-2$ delay units and N multipliers, and the computation cost is the same as that of an ordinary $2N-1$ order linear phase filter.

In this paper, adaptive threshold algorithm is used to determine the location of notch frequency points. The spectrum value without NBI is usually set as the minimum threshold $Thre_{\min}$, then the threshold is determined by an adaptive method

$$Thre = Thre_{\min} + \eta \frac{1}{N_{FFT}} \sum_{\lambda=1}^{N_{FFT}} abs(V_\lambda) \tag{28}$$

where N_{FFT} is the point of FFT, η is threshold optimization coefficient, which is chosen from the preset set according to $\frac{1}{N_{FFT}} \sum_{\lambda=1}^{N_{FFT}} abs(V_\lambda)$. And V_λ is FFT output of input signal after all-phase processing

$$V_\lambda = \sum_{n=1}^{N_{FFT}} r(n) w_r(n) e^{-j2\pi n\lambda/N_{FFT}} \quad \lambda = 1, \ldots, N_{FFT} \tag{29}$$

where $w_r(n)$ is general window function. The interference threshold *Thre* is obtained in Equation (28). It is generally considered that the spectral lines containing NBI are those whose spectral values are greater than the interference threshold *Thre*. By determining the position of these interference lines (the smaller the range is, the more accurate μ and l are), notch was carried out in the apFIR filter and then Inverse Fast Fourier Transform (IFFT) was used to obtain the time-domain signal after NBI suppressing.

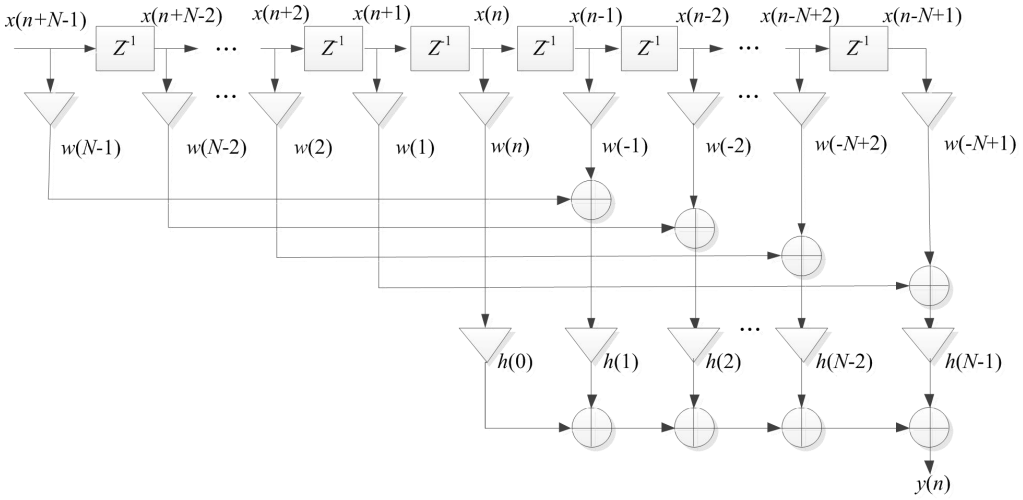

FIGURE 2. The structure of a single-window apFIR filter.

C. AN IMPROVED PMF-FFT ALGORITHM BASED-ON ALL-PHASE PROCESSING

After NBI suppression, the signal $b(i)$ with length of L is cut into R parts, each part has P points, i.e. $L = RP$. When PN code phase of the received signal is aligned with the local PN phase, the output of rth $(1 \le r \le R)$ PMF is shown by

$$\begin{aligned} x_{\mathrm{PMF}} &= \frac{1}{P} \sum_{i=(r-1)P+1}^{rP} b(i)s(i+i') \\ &= \frac{1}{P} \frac{\sin(\pi P f_d T_c)}{\sin(\pi f_d T_c)} \exp\left[j\pi f_d T_c (2rP - P) + \phi\right] \end{aligned} \tag{30}$$

where i' is the delay between the local PN code and the received PN code, ϕ is the phase of signal after IFFT.

Applying all-phase preprocessing and Q points FFT to x_{PMF}, normalized output frequency response can be expressed as

$$\begin{aligned} G_{ap}(f_d, k) &= \frac{1}{Q^2} \sum_{m=0}^{Q-1} \sum_{i=0}^{Q-1} x(m-i) e^{-j\frac{2\pi}{Q}km} e^{j\frac{2\pi}{Q}ki} \\ &= \frac{1}{Q^2} e^{-j\pi P f_d T_c + \varphi} \cdot \frac{1}{P} \frac{\sin(\pi P f_d T_c)}{\sin(\pi f_d T_c)} \\ &\quad \cdot \sum_{m=0}^{Q-1} e^{-j(2\pi P f_d T_c - k)m/Q} \cdot \sum_{r=0}^{Q-1} e^{j(2\pi P f_d T_c - k)i/Q} \\ &= \frac{1}{LQ^2} \cdot e^{j\phi_{\text{PMF-apFFT}}(f_d,k)} \frac{\sin(\pi P f_d T_c)}{\sin(\pi f_d T_c)} \\ &\quad \cdot \frac{\sin^2\left(\pi L f_d T_c - \pi Rk/Q\right)}{\sin^2\left(\pi P f_d T_c - \pi k/Q\right)}, \\ &\qquad k = 0, 1, \ldots, N-1 \\ &= G_1(f_d, k) \times G_2(f_d, k) e^{j\phi_{\text{PMF-apFFT}}(f_d,k)} \end{aligned} \tag{31}$$

where

$$\phi_{\text{PMF-apFFT}}(f_d, k) = -\pi f_d (P-1) T_c + 2\pi N (f_d P T_c - k/Q) \tag{32}$$

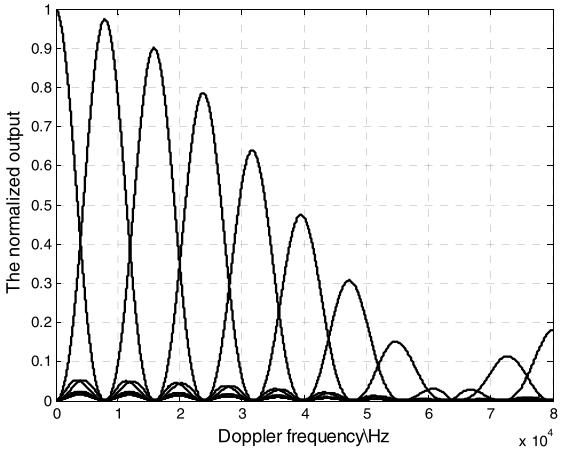

FIGURE 3. The output of PMF-apFFT with different Doppler frequencies.

$$G_1(f_d, k) = \frac{1}{L} \frac{\sin(\pi P f_d T_c)}{\sin(\pi f_d T_c)} \tag{33}$$

$$G_2(f_d, k) = \frac{1}{Q^2} \frac{\sin^2(\pi L f_d T_c - \pi Rk/Q)}{\sin^2(\pi P f_d T_c - \pi k/Q)} \tag{34}$$

According to Equation (31), the normalized output of PMF-apFFT acquisition algorithm consists of $G_1(f_d, k)$ and $G_2(f_d, k)$. $G_1(f_d, k)$ is introduced by the accumulation of PMF, with the increase of Doppler frequency, it results in periodic attenuation of FFT output, i.e. scallops loss, known as fan effect. Figure 3 is the simulation chart of Equation (31) taking Doppler frequency as x-axis and 8-point FFT. $G_2(f_d, k)$ is caused by incomplete FFT phase compensation, and it can be seen as the compensation term of apFFT, which is the square of that of common FFT, and energy of the side lobe relative to energy of the main lobe is attenuated according to such a quadratic relationship [20]. Therefore, apFFT algorithm has a better performance in reducing spectrum leakage.

D. DETECTION PROBABILITY

In the additive white Gaussian noise environment, false alarm and missed detection occur in the acquisition, H_0 denotes the noise signal, H_1 denotes the presence of useful signal. The probability of false alarm depends on the distribution characteristics of the input noise, and the output of a single frequency channel is subject to Rayleigh distribution after apFFT, its mean $m_a = 0$ and variance $\sigma^2 = (2N^2+1)\sigma_n^2/3N$, so the probability density function of single channel's output is shown by [20]

$$P_{Rayleigh}(a) = \frac{a^2}{\sigma^2}\exp\left(-\frac{a^2}{2\sigma^2}\right), \quad a \geq 0 \tag{35}$$

Due to statistical independence for each channel, it is equivalent to the N-Tuple Bernoulli experiment, which is subject to the Binomial distribution, the probability of any one of Q outputs exceeding the threshold (the probability of false alarm) in the system can be expressed as

$$p_{fa} = 1 - \left[1 - p_a(\overline{\mathbf{X}_{ap}} > V_T|H_0)\right]^Q \tag{36}$$

The expression of threshold V_t can be obtained from Eq.(36)

$$V_t = \sqrt{-2L\ln\left[1-\left(1-p_{fa}\right)^{1/Q}\right]} \tag{37}$$

And the probability of false alarm P_a in a single channel can be expressed as

$$P_a = \int_{V_t}^{+\infty}\frac{x^2}{\sigma^2}\exp\left(-\frac{a^2}{2\sigma^2}\right)da = \exp\left(-\frac{V_t^2}{2\sigma^2}\right) \tag{38}$$

At the output of the apFFT, the amplitude of the signals are taken, thus the statistics of the output of some apFFT bin k are Ricean, is given by

$$P_{Rician}(a) = \frac{a}{\sigma_n^2}\exp\left(-\frac{a^2+m^2}{2\sigma_n^2}\right)I_0\left(\frac{am}{\sigma_n^2}\right), \quad a \geq 0 \tag{39}$$

where I_0 is the zero-order modified Bessel function, and m is the summation of the mean of the signals on the inphase and quadrature branches for bin k

$$m^2 = m_I^2 + m_Q^2 \tag{40}$$

The detection probability of the kth channel can be expressed as

$$\begin{aligned} P_d(k) &= p_{Rician}\left(X_{ap}(k) > V_T|H_1\right) \\ &= \int_{V_t}^{+\infty} P_{Rician}(a)da = \mathrm{Q}\left(m/\sigma, V_t/\sigma\right) \\ &= \mathrm{Q}\left(\sqrt{6XN^2/\left(2N^2+1\right)\cdot\left|G_{ap}(k)\right|}, \right. \\ &\quad \left.\sqrt{-2\ln\left(1-N\sqrt{1-P_{fa}}\right)}\right) \end{aligned} \tag{41}$$

where $\mathrm{Q}(\cdot)$ is Marcumq function. Signal acquisition is assumed if any of the output bins is greater than the threshold. Each of the Q FFT output bins have the same distribution, and therefore the probability of any one of the Q outputs exceeding the threshold can be given by

$$P_d = 1 - \prod_{k=0}^{Q-1}\left(1 - P_d(k)\right) \tag{42}$$

where P_d is detection probability of the proposed algorithm in the Gaussian channel.

III. THE STEPS OF THE PROPOSED ALGORITHM

The process is as follow

1) After down conversion and analog-digital conversion (ADC), the contaminated BOC signal $z(t)$ is converted to its discrete signal $\mathbf{x}$.

2) The notch point range is determined according to the amplitude larger than the *Thre*, which is generated by the adaptive threshold algorithm shown in Equation (28).

3) The apFIR filter is designed according to the parameters obtained in step 2, $b(i)$ is obtained by apFIR filter and IFFT.

4) The signal $b(i)$ and local BOC baseband signal are taken L points in order and cut into R parts, and each part has P points.

5) The signal $b(i)$ is correlated with the local BOC baseband signal in each segment by PMF, and R segments are completed successively.

6) The output of PMF $\mathrm{x_{PMF}}$ is done by all-phase preprocessing and N points FFT. The maximum value of the result is compared with the threshold V_t. If the maximum value exceeds the threshold V_t, the receiver enters the tracking stage; if not, by logic control, the first segment of the local BOC baseband signal is deleted, and the remaining $R-1$ segments are moved forward in turn, and then a sequence of data is added in the following order.

7) The steps 4-6 are repeated until the value of peak exceeds the threshold.

Figure 4 describes steps of the proposed algorithm.

IV. SIMULATION AND RESULTS ANALYSIS

In this paper, the performance of apFIR filter and the acquisition algorithm are simulated in MATLAB, Hamming window is adopted in all-phase spectrum analysis and traditional FFT spectrum analysis. If no otherwise specified, sinBOC(1,1) modulated signal is simulated in additive white Gaussian noise channel, and simulation parameters are set as follows. The received BOC signal is mixed with two single-tone interference signals, whose angular frequencies are 0.3 rad/s and 0.5 rad/s, respectively. The length of frequency vector $\mathbf{H}$ $M = 16$, Doppler frequency $f_d = 6$kHz, the PN code rate is 8.148MHz. The length of partial matched filter $P = 255$, the number of partial matched filter $R = 4$, the length of BOC modulated baseband signal $L = P^*R = 1020$, the number of FFT $N = 128$. And integral time $T = 1$ms, false alarm probability $P_{fa} = 0.01$, threshold optimization coefficient

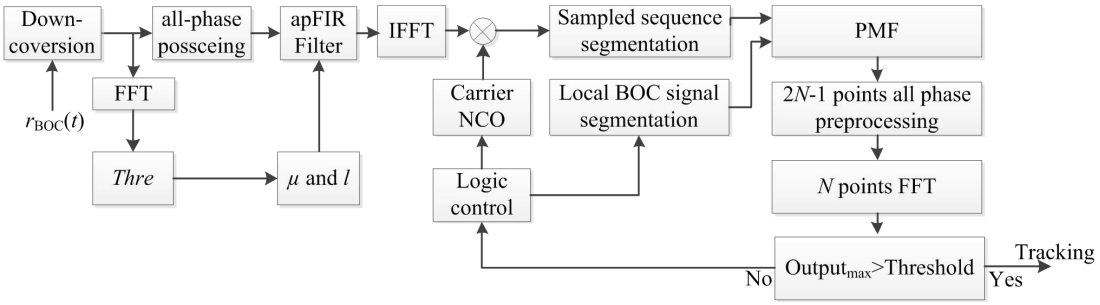

FIGURE 4. The block diagram of the proposed algorithm.

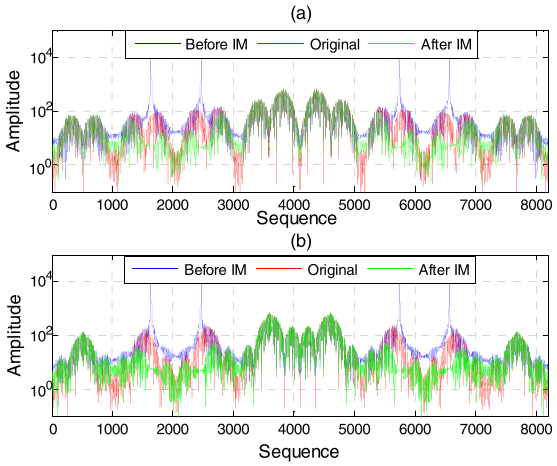

FIGURE 5. The comparison of the spectrum of original signal and signals before and after IM. (a) cosBOC(1,1); (b) sinBOC(2,1).

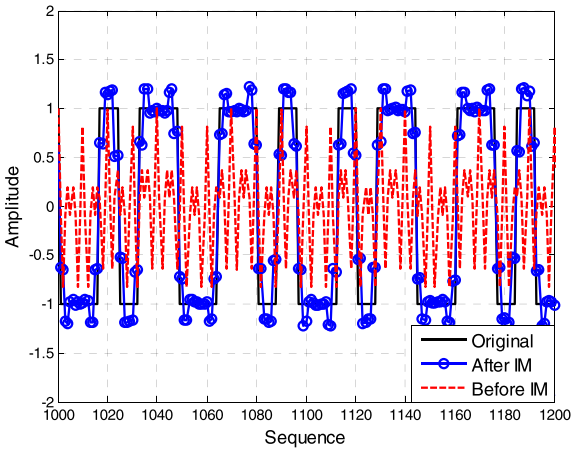

FIGURE 6. The comparison of the waveform of original signal and signals before and after IM for cosBOC(1,1).

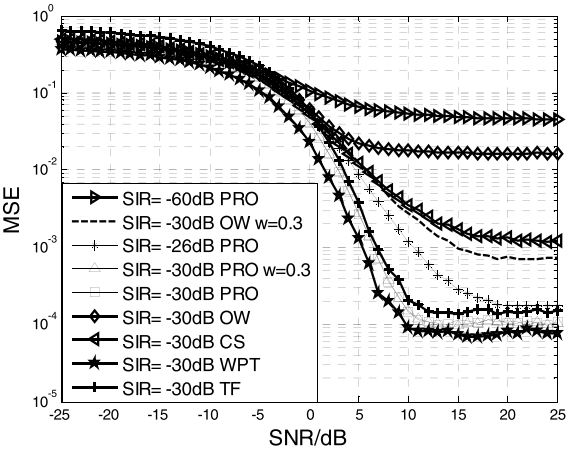

FIGURE 7. MSE in different conditions.

$\eta = 5$ and signal to interference ratio (SIR) is -30dB, signal to noise ratio (SNR) is 2dB.

A. SIGNAL SPECTRUM AND SIGNAL WAVEFORM

In Figure 5a and Figure 5b, Four spectral lines with abnormally high amplitude are caused by NBI, respectively. Compared with the spectrum of original signal, the spectrum of signal after interference mitigation (IM) has less distortion, and the amplitude of the spectral lines where interference signals located is effectively reduced. It can be seen that the NBI is effectively suppressed and the received signal can be basically recovered. In addition, the proposed algorithm is suitable for all modulation orders sinBOC and cosBOC.

To further analyze the effect of the proposed anti-jamming method, three sections of cosBOC(1,1) signals are intercepted in Figure 6, in which the amplitude of signal before IM is normalized. It can be seen clearly that NBI has a serious impact on the waveform of BOC baseband signal. By comparing the time-domain signals before and after IM and the original signal, the influence of NBI on BOC signal is greatly weakened by apFIR filter. Obviously, with the further reduction of SIR, BOC signal will obviously suffer serious loss and energy leakage.

B. MEAN SQUARE ERROR

The quality of a retrieved signal is determined through its mean square error (MSE)

$$\mathrm{MSE} = \frac{1}{K}\sum_{k=1}^{K}\left[\hat{r}\,(k) - r\,(k)\right]^2 \tag{43}$$

where $\hat{r}\,(k)$ is the retrieved BOC signal.

In Figure 7, the ability of the proposed method for mitigating jamming is best when SIR $= -30$dB, as the jamming

intensity decreases (SIR $= -26$dB), *Thre* decreases as well, and the useful signal exceeding the *Thre* is also suppressed, which makes MSE large. In addition, MSE of proposed algorithm is lower than that of CS, OW and TF (TF is Time-Frequency domain algorithm proposed in [10]) algorithm and slightly higher than that of WPT algorithm in the same condition, which shows that the proposed algorithm has a good performance in NBI anti-jamming. Comparing the two curves of OW algorithm, it can be seen that there is a large additional loss in OW algorithm, as the interference frequency is not an integral multiple of the frequency resolution. The curve of two single-tone jamming signals of 0.3 rad/s and 0.5 rad/s, coincides with the curve of one single-tone jamming signal of 0.3 rad/s, which shows that the number of jamming signals and frequency angles of jamming signals have no effect on the proposed anti-jamming algorithm.

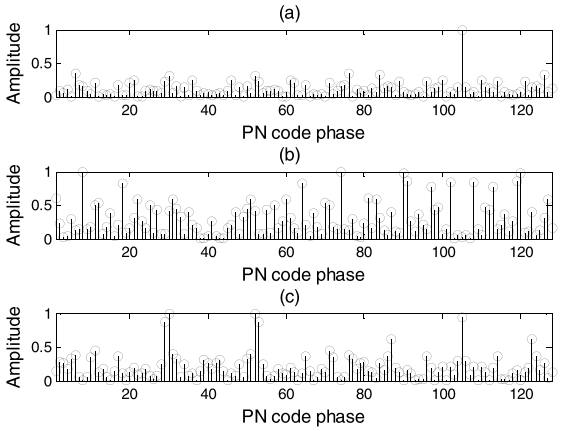

FIGURE 8. The normalized amplitudes of PMF-apFFT algorithm. (a) PMF-apFFT algorithm with IM; (b) PMF-apFFT algorithm without IM; (c) PMF-FFT algorithm with IM.

C. SIMULATION OF THE PROPOSED ALGORITHM

The normalized outputs of different algorithms in Figure 8 are obtained by 100 times simulations for averaging. Figure 8a shows that the main peak of the proposed algorithm for the contaminated BOC signal is obvious. However, NBI makes the output of PMF-apFFT algorithm without IM confused and causes the position of the main peak cannot be found in Figure 8b. Compared Figure 8a with Figure 8c, it shows that the main peak of PMF-apFFT algorithm is more obvious than that of PMF-FFT algorithm, which makes it easier to detect the location of the main peak.

Figure 9 demonstrates the estimation of Doppler frequency obtained by 100 times simulations for averaging with and without IM, respectively. As it can be understood from Figure 9a and Figure 9b, the impact of the proposed algorithm on narrowband anti-jamming is obvious and the peak appears at 6062 Hz, which is almost consistent with the previous Doppler frequency set of 6KHz. Combined with Figure 8 and Figure 9, it is concluded that the proposed algorithm can achieve the two-dimensional acquisition of code phase and Doppler frequency.

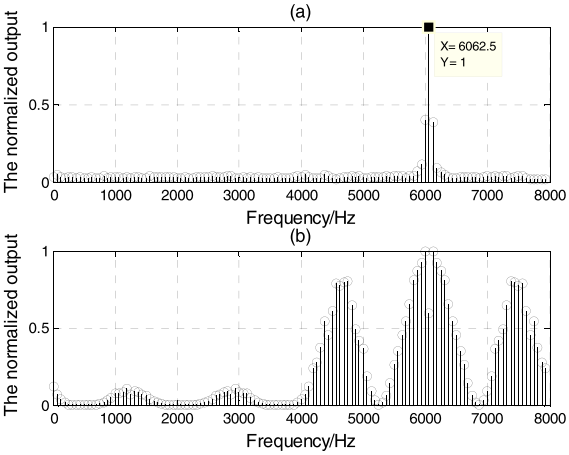

FIGURE 9. The Doppler frequency estimations of PMF-apFFT algorithm. (a) With IM. (b) Without IM.

D. DETECTION PROBABILITY

To further evaluate the impact of narrowband anti-jamming technique on the performance of acquisition unit, curves of detection probabilities under different working conditions are assessed by Monte Carlo simulations in Figure 10. If no otherwise specified, PMF-apFFT is adopted for acquisition. When SIR $= -30$dB, detection probability of the proposed algorithm reaches 1 at SNR $= 1.5$dB, which is better than that of OW, CS, TF and apFIR&PMF-FFT algorithm but worse than that of WPT algorithm. In addition, detection probability of the proposed algorithm for cosBOC(1,1) is also obtained in Figure 10. Without apFIR filter, detection probability is always zero, no matter how the SNR increase. As the SIR decreases to -60dB, the detection probability of proposed algorithm decreases by 3.5dB. It is to be noted that as the MSE of the retrieved signal decreases, the quality of this signal increases. Therefore, the results obtained in Figure 10 correspond to the results in Figure 7.

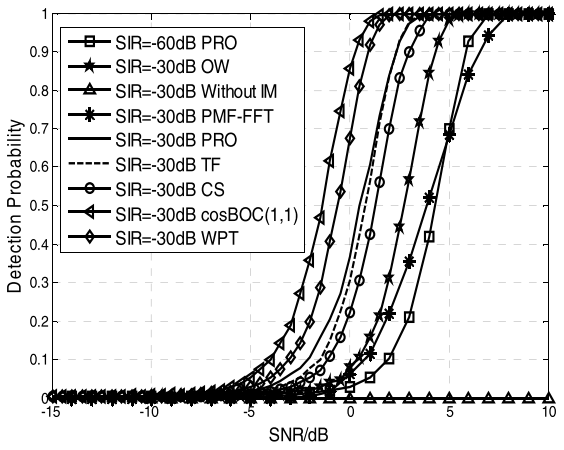

FIGURE 10. Detection Probabilities for different algorithms.

TABLE 1. The calculations of FFT and windowless apFFT.

Algorithm	data length	Ord -er	Complex multiplication	Complex addition	Real addition
FFT	O	O	$(O/2)\log_2 O$	$O\log_2 O$	-
Windowless apFFT	$2O$-1	O	$(O/2)\log_2 O$	$O\log_2 O$	$O(O$-1)

E. CALCULATION AND HARDWARE REQUIREMENT

ApFFT is to add the all phase processing to the data before FFT. Therefore, compared with FFT, more calculation is on the windowing and summation of data in all phase processing, and windowless apFFT only carries out $O(O$-1) real addition to data. In general, for O points apFFT, double window, single window and windowless apFFT all do approximately O^2 more real addition than FFT, and they do the same amount of complex multiplication and addition, which are shown in Table.1. Due to the calculation of single addition is much smaller than that of single multiplication, so the added amount of real addition operations is small compared with the total amount of computation. In addition, $2O$-1 points data is required for O points apFFT and segmented from back to front, so apFFT cannot be carried out until $2O$-1 data is in place, and FFT can be carried out as long as O data are in place, so apFFT requires almost twice as much storage as that of FFT. However, compared with the good performance of spectrum analysis of apFFT, the increased hardware cost is acceptable. Due to the complexity and large calculation of WPT and CS algorithm, the costs of system resources and storage are large. Although the implementation of TF algorithm is simple, it is limited by the convergence speed, so the real-time performance of the proposed algorithm is better than that of WPT, CS and TF algorithms.

V. CONCLUSION

In this paper, the problem of BOC signal acquisition with NBI was studied, and a novel acquisition algorithm combining apFIR filter and PFM-apFFT is proposed. The apFIR filter is simple in structure and easy to be implemented, and the range of notch can be adjusted by the parameters l and μ according to the adaptive threshold algorithm. PMF-apFFT algorithm employs all-phase FFT to reduce spectrum leakage, which further improves the acquisition performance. The proposed algorithm can effectively suppress NBI and basically recover the original signal waveform and spectrum. And it has a excellent performance in the terms of MSE and detection probability. In addition, compared with existing typical algorithms, the proposed algorithm has moderate calculation and hardware requirements. For the characteristics of the proposed algorithm, it is suitable for the system with high real-time requirements and low SIR, and it can be adopted in fast-moving receiver or other communications system suffering from NBI.

TABLE 2. Symbol check list.

Symbol	Meaning	Symbol	Meaning
A	Signal amplitude	O	The length of input data
C	Normalization factor	P	The length of PMF
$\mathbf{D}$	Data matrix	Q	FFT points
f_{IF}	Intermediate frequency	R	The number of PMF
f_{sc}	Subcarrier frequency	T_c	The period of PN code
f_d	Doppler frequency	T_{sc}	The period of subcarrier
G_{ap}	Frequency response	$Thre$	Interference threshold
$\mathbf{H}$	Frequency vector	μ	Notch parameter
K	The number of single-tone jamming	V_t	Acquisition threshold
l	Notch parameter	$\mathbf{x}$	The sampled data vector
M	The length of $\mathbf{H}$	$\mathbf{x}_{ap}$	The all-phase vector
N	The length of $\mathbf{x}_{ap}$	x_{PMF}	The output of PMF

APPENDIX

See Table 2.

ACKNOWLEDGMENT

This research is supervised by Tianqi Zhang and Gang Zhang from Chongqing University of Posts and Telecommunications. Thanks also go to the authors of the papers mentioned in Reference.

REFERENCES

[1] H. Xiong, S. Wang, S. Gong, M. Peng, J. Shi, and J. Tang, "Improved synchronisation algorithm based on reconstructed correlation function for BOC modulation in satellite navigation and positioning system," *IET Commun.*, vol. 12, no. 6, pp. 743–750, Apr. 2018.
[2] O. Julien, C. Macabiau, M. E. Cannon, and G. Lachapelle, "ASPeCT: Unambiguous sine-BOC(n,n) acquisition/tracking technique for navigation applications," *IEEE Trans. Aerosp. Electron. Syst.*, vol. 43, no. 1, pp. 150–162, Jan. 2007.
[3] J. Long, C. Yang, and F. Lin, "Pseudo correlation function based ambiguity mitigating technique for cosine-phased BOC signals," in *Proc. Int. Conf. Adv. Technol. Commun. (ATC)*, Ho Chi Minh City, Vietnam, Oct. 2013, pp. 569–573.
[4] Z. Yao, X. Cui, M. Lu, Z. Feng, and J. Yang, "Pseudo-correlation-function-based unambiguous tracking technique for sine-BOC signals," *IEEE Trans. Aerosp. Electron. Syst.*, vol. 46, no. 4, pp. 1782–1796, Oct. 2010.
[5] M. Elgenedy, M. M. Awadin, R. Hamila, W. U. Bajwa, A. S. Ibrahim, and N. Al-Dhahir, "Sparsity-based joint NBI and impulse noise mitigation in hybrid PLC-wireless transmissions," *IEEE Access*, vol. 6, pp. 30280–30295, 2018.
[6] D. Borio, H. Li, and P. Closas, "Huber's non-linearity for GNSS interference mitigation," *Sensors*, vol. 18, no. 7, pp. 2217–2229, 2018.
[7] H. Xiong, "An efficient narrowband interference suppression approach in ultra-wideband receiver," *IEEE Sensors J.*, vol. 17, no. 9, pp. 2741–2748, May 2017.

[8] K. Kikuta and A. Hirose, "Narrowband interference mitigation in UWB systems utilizing frequency dependence of null formation in array antennas," *IEEE Access*, vol. 4, pp. 8715–8720, 2016.
[9] S. Daneshmand, T. Marathe, and G. Lachapelle, "Millimetre level accuracy GNSS positioning with the blind adaptive beamforming method in interference environments," *Sensors*, vol. 16, no. 11, pp. 1824–1840, 2016.
[10] M. Villanti, R. Pedone, G. E. Corazza, and R. Crescimbeni, "Joint time-frequency domain interference mitigation for Galileo L1 band receivers," in *Proc. IEEE 9th Int. Symp. Spread Spectr. Techn. Appl.*, Aug. 2006, pp. 238–242.
[11] J. W. Betz, "Effect of narrowband interference on GPS code tracking accuracy," in *Proc. Nat. Tech. Meeting Inst. Navigat.*, Anaheim, CA, USA, Jan. 2000, pp. 16–27.
[12] M. Abedi, M. J. Rezaei, and M. R. Mohammad, "Accurate interference mitigation in global positioning system receivers based on double-step short-time Fourier transform," *Circuits, Syst., Signal Process.*, vol. 37, no. 6, pp. 2450–2470, 2018.
[13] L. Musumeci and F. Dovis, "Use of the wavelet transform for interference detection and mitigation in global navigation satellite systems," *Int. J. Navigat. Observ.*, vol. 2014, pp. 1–14, Feb. 2014.
[14] S. Liu, F. Yang, W. Ding, X. Wang, and J. Song, "Two-dimensional structured-compressed-sensing-based NBI cancelation exploiting spatial and temporal correlations in MIMO systems," *IEEE Trans. Veh. Technol.*, vol. 65, no. 11, pp. 9020–9028, Nov. 2016.
[15] S. Liu, F. Yang, W. Ding, and J. Song, "Double kill: Compressive-sensing-based narrow-band interference and impulsive noise mitigation for vehicular communications," *IEEE Trans. Veh. Technol.*, vol. 65, no. 7, pp. 5099–5109, Jul. 2016.
[16] M. J. Medley, G. J. Saulnier, and P. K. Das, "Narrow-band interference excision in spread spectrum systems using lapped transforms," *IEEE Trans. Commun.*, vol. 45, no. 11, pp. 1444–1455, Nov. 1997.
[17] M. Tanabe, A. Saito, M. Umehira, and S. Takeda, "A novel overlap FFT filter-bank using windowing and smoothing techniques to reduce adjacent channel interference for flexible spectrum access," in *Proc. Int. Conf. Inf. Commun. Technol. Converg. (ICTC)*, Oct. 2016, pp. 115–120.
[18] Z. X. Hou, Z. H. Wang, and X. Yang, "Design and implementation of all phase DFT digital filter," *Acta Electronica Sinica*, vol. 31, no. 4, pp. 539–543, 2003.
[19] J. Tian, J. Sun, G. Wang, Y. Wang, and W. Tan, "Multiband radar signal coherent fusion processing with IAA and apFFT," *IEEE Signal Process. Lett.*, vol. 20, no. 5, pp. 463–466, May 2013.
[20] X.-D. Huang and Z.-H. Wang, "Anti-noise performance of all-phase FFT phase measuring method," *J. Data Acquisition Process*, vol. 26, no. 3, pp. 286–291, 2011.

YI PAN was born in 1988. He received the B.S. degree and M.S. degree in signal and information processing from the Chongqing University of Posts and Telecommunications, in 2011 and 2014, respectively, where he is currently pursuing the Ph.D. degree in signal and information processing. His research interests include spread spectrum signal detection and processing, acquisition, tracking of BOC signal, and interference mitigating.

TIANQI ZHANG was born in 1971. He received the B.S. degree in physics from the Southwest University of China, in 1994, and the M.S. degree in communication and electronic system and the Ph.D. degree in circuits and systems from the University of Electronic Science and Technology of China, in 1997 and 2003, respectively. From 2003 to 2005, he was a Postdoctoral Fellow in communication and information system with Tsinghua University, and majors. Since 2005, he has been a Professor of the School of Communication and Information Engineering, Chongqing University of Posts and Telecommunications. His research interests are in areas of communication, and image and speech signal processing.

GANG ZHANG was born in 1976. He received the Ph.D. degree from the College of Communication Engineering, Chongqing University, Chongqing, in 2009. He is currently a Professor at Chongqing University of Posts and Telecommunication. His research interests involve chaotic synchronization, chaotic secure communication, and weak signal detection.

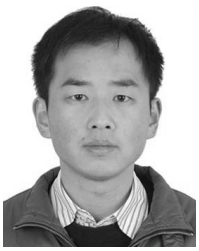

ZHONGTAO LUO received the M.S. degree in electronic engineering and the Ph.D. degree in signal and information processing from the University of Electronic Science and Technology of China, Chengdu, in 2007 and 2015, respectively. He is currently a Lecture with the Chongqing University of Posts and Telecommunication. His research interests include statistical signal processing, array signal processing, and their applications in radar and communication systems.